

Nonlinear optical response as a probe of emergent Lorentz symmetry violation in noncentrosymmetric materials

Guilherme J. Inacio,^{1,2} Nathanael N. Batista,¹ Wesley Spalenza,^{3,4}
Humberto Belich,¹ Juan José Palacios,^{2,5,6} and Wendel S. Paz^{1,2,*}

¹Departamento de Física, Universidade Federal do Espírito Santo, 29075-910 Vitória-ES, Brazil

²Departamento de Física de la Materia Condensada,

Universidad Autónoma de Madrid, E-28049 Madrid, Spain

³Instituto Federal do Espírito Santo, IFES - Cariacica, ES, Brasil

⁴Centro Brasileiro de Pesquisas Físicas, CBPF, RJ, Brasil

⁵Condensed Matter Physics Center (IFIMAC), Universidad Autónoma de Madrid, E-28049 Madrid, Spain

⁶Instituto Nicolás Cabrera (INC), Universidad Autónoma de Madrid, E-28049 Madrid, Spain

(Dated: January 21, 2026)

We propose an electrically controlled protocol to detect weak Lorentz-violating (LV) backgrounds through the second-order shift photocurrent in noncentrosymmetric crystals. Using a spinful Rice–Mele model, we show that a stationary LV background induces a momentum-odd correction to the Bloch Hamiltonian, which generates an odd-in-field contribution to the shift current. This leads to a directional asymmetry, whereby the photocurrent distinguishes opposite orientations of an applied static field. The effect originates from an LV-induced deformation of the interband phase and can be isolated experimentally by comparing field-reversed configurations, with vanishing response at transverse orientations, providing an internal consistency check. Our results demonstrate that nonlinear optical responses offer a practical and symmetry-selective route for probing LV effects in solid-state systems.

Lorentz symmetry plays a central role in modern physics because it ensures that the laws of nature do not depend on orientation or uniform motion. Within the Standard-Model Extension (SME) this symmetry can be relaxed in a controlled way by allowing matter and gauge fields to couple to fixed background tensors, leading to small deviations from exact Lorentz and CPT invariance [1–4]. A broad range of precision experiments has used this framework to place tight bounds on possible deviations, including tests based on cavity resonators, atomic spectroscopy, spin-precession measurements, and astrophysical observations [5–10]. Condensed matter systems offer a complementary perspective because their low-energy quasiparticles can display relativistic features. In Weyl and Dirac semimetals for example, tilted dispersions and parity-odd responses mimic effective Lorentz-violating (LV) terms [11–15], and non-minimal SME-inspired couplings can generate Rashba-type interactions and modified Landau levels in crystalline Hamiltonians [16–18]. Yet, the influence of actual LV backgrounds on physical observables in the context of condensed matter physics remains largely unexplored.

Nonlinear photocurrents, and especially the shift current, are known to be highly sensitive to the phase structure and Berry geometry of Bloch states in crystals that lack inversion symmetry [19–23]. These responses have been measured with high precision in a variety of low-dimensional semiconductors, including transition-metal dichalcogenide nanoribbons, nanotubes, ferroelectric layers, and flexo-photovoltaic devices [24–29]. Their sensitivity and experimental maturity make them ideal tools for detecting subtle symmetry-breaking perturba-

tions that modify band geometry.

In this work, we propose a viable device configuration to probe LV backgrounds through a directional asymmetry of the shift photocurrent in a noncentrosymmetric nanowire. The setup consists of an elongated, electrically biased wire illuminated by monochromatic light, where the photocurrent is measured along the wire axis while the orientation of an applied static electric field is reversed, like illustrated in Figure 1. To capture the essential physics in a minimal and controlled setting, we model the nanowire using a spinful Rice–Mele lattice Hamiltonian supplemented by a weak LV-induced perturbation. This background field generates a momentum-odd correction to the Bloch Hamiltonian, which alters the phase structure of the interband optical matrix elements. As

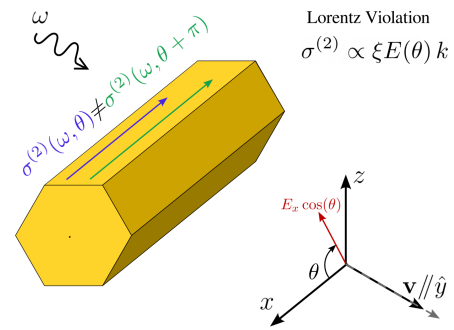


FIG. 1. Proposed angular-resolved setup for detecting LV signatures in the shift current. Opposite field orientations (θ and $\theta + \pi$) yield unequal photocurrents in the presence of a momentum-odd LV perturbation.

a consequence, the shift current acquires a component that is odd under reversal of the applied static field, leading to a measurable difference between photocurrents obtained for opposite field orientations. The resulting field-directional asymmetry provides a direct and experimentally accessible signature of LV-induced band-geometry deformation, which can be isolated by comparing measurements taken under field reversal while keeping the sample and optical geometry fixed.

Theory — LV effects can persist in the non-relativistic limit, as shown by Kostelecký and Lane [30], and they motivate a variety of effective Hamiltonians in both high-energy physics and condensed matter [11–15, 18, 31]. To capture the essential mechanism by which a LV background affects the band geometry and the nonlinear optical response, we employ a one-dimensional lattice model that provides a simple and controlled setting. We start from a Dirac equation modified by a non-minimal coupling to a fixed background four-vector v^μ [32–36]. After a Foldy-Wouthuysen reduction, the non-relativistic Hamiltonian contains orbital and spin terms proportional to the background field [17, 37]. These couplings are known to give rise to Rashba-like and Zeeman-like contributions in the effective Hamiltonian of non-relativistic electrons,

$$H_{\text{LV}} = \frac{g}{2m_e} \boldsymbol{\sigma} \cdot \left[\nabla \times \left(\mathbf{v} \times \frac{\mathbf{E}}{c} \right) \right] - \frac{g}{m_e} \mathbf{p} \cdot (\mathbf{v} \times \mathbf{E}), \quad (1)$$

where the first term acts on the spin component and the second on the orbital channel and together provide the basic structure from which the lattice model is constructed. To this aim, we project this Hamiltonian onto the RM basis [38], associated with a one-dimensional chain with staggered hoppings and on-site potentials,

$$H_{\text{RM}}(k) = [d_x(k)\tau_x + d_y(k)\tau_y + d_z\tau_z] \otimes \sigma_0, \quad (2)$$

with hopping elements

$$d_x(k) = t_1 + t_2 \cos(ak), \quad (3)$$

$$d_y(k) = -t_2 \sin(ak), \quad (4)$$

$$d_z = \Delta, \quad (5)$$

where a is the lattice constant, t_1 and t_2 are the intra-cell and intercell hopping parameters, τ_i acts in sublattice space, and σ_i act on real spin. For a chain oriented along \hat{x} we treat the background \mathbf{v} as a static transverse field, v_y , and the optical drive as an electric field with longitudinal component E_x . In this configuration, the non-minimal coupling generates a low-energy, inversion-symmetric correction of the form

$$H_{\text{LV}}(k) = \lambda_k \left(\tau_y \otimes \sigma_0 + \frac{1}{2} \tau_y \otimes \sigma_y \right), \quad (6)$$

with $\lambda_k = \alpha k$, $\alpha = \hbar\xi E_x/(m_e c)$ and $\xi = gv_y$. The term proportional to $\tau_y \otimes \sigma_0$ provides the orbital tilt induced by

the background field, and the weaker term proportional to $\tau_y \otimes \sigma_y$ encodes the Rashba-like coupling predicted in LV models [37]. Although small, the spin channel lifts the degeneracy of the bands and ensures that the Bloch states acquire smooth phases across the Brillouin zone. Projecting the continuum LV correction onto the two-sublattice RM basis yields a k -odd modification of the intercell hopping, which in Bloch form enters the sublattice sector through a τ_y structure. The explicit reduction and projection are given in Supplementary Material S1. The full Hamiltonian thus becomes

$$H_{\text{eff}}(k) = H_{\text{RM}}(k) + H_{\text{LV}}(k). \quad (7)$$

The eigenstates from the Hamiltonian determine the interband dipoles and shift vectors entering the length-gauge expression for the second-order shift conductivity [19–21, 23],

$$\begin{aligned} \sigma_{ab}^{(2)}(\omega, \theta) = & \quad (8) \\ & - \frac{\pi e^3}{\hbar^2} \sum_{m,n} \int \frac{dk}{2\pi} f_{mn}(k) R_{mn}^a(k) |r_{mn}^b(k)|^2 \delta(E_{mn} - \omega). \end{aligned}$$

Given that the system is one-dimensional, with both the electronic dispersion and the light-matter coupling confined to the chain direction \hat{x} , the only nonvanishing component of the nonlinear conductivity tensor is the longitudinal one, $\sigma_{xxx}^{(2)}$. Thus, this is the component evaluated in this work and shown in Figure 2.

Because the LV perturbation (LVP) is odd in k and enters the inter-sublattice hopping channel through τ_y , it reshapes the complex phase of the Bloch spinors and therefore the phase $\phi_{mn}(k)$ of the interband dipole matrix elements. This induces a k -odd contribution to the shift vector $R_{mn}^a(k)$ and, consequently, an E_x -odd component of the shift conductivity. The LV coupling depends on the cross product $\mathbf{v} \times \mathbf{E}$ between the fixed background vector \mathbf{v} and an externally applied static electric field \mathbf{E} . Upon rotating \mathbf{E} by an angle θ , only its longitudinal projection $E_x(\theta) = E_0 \cos \theta$ contributes to H_{LV} , so that reversing the field orientation, $\theta \rightarrow \theta + \pi$, flips the sign of the LV contribution while leaving the even background unchanged. As a result, the conductivity does not need to satisfy $\sigma^{(2)}(\omega, \theta) = \sigma^{(2)}(\omega, \theta + \pi)$, and the resulting π -odd provides the primary experimental signature of the LV background. Details of the gauge fixing, numerical stabilization, and implementation are given in Supplementary Material S2.

Results — To analyze the directional response induced by the LV background, we evaluate the shift conductivity as a function of the incidence angle θ of the applied static electric field, as shown in Fig. 2. The calculations use a one-dimensional k mesh with $N_k = 5001$, a Gaussian broadening $\eta = 0.015\text{eV}$, a static background field $E_x = 10^5 \text{ V m}^{-1}$ ($= 1 \text{ kV cm}^{-1}$), well within experimentally accessible bias field strengths [39–43]. Lastly,

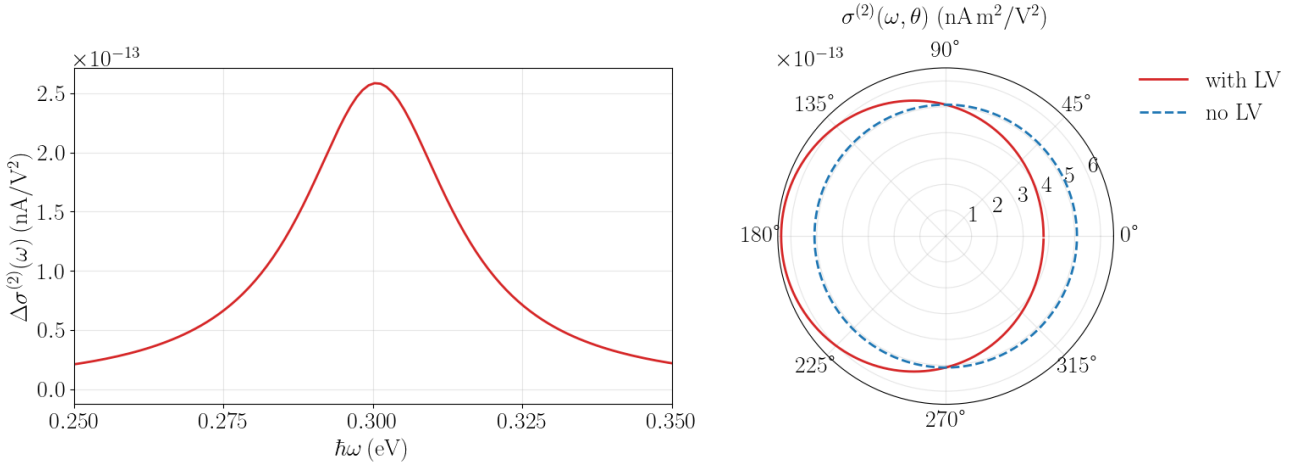


FIG. 2. Left: Difference $\Delta\sigma^{(2)}(\omega) = \sigma^{(2)}(\omega, \theta = \pi) - \sigma^{(2)}(\omega, \theta = 0)$, showing a peak contrast of $1.53 \text{ nm} \cdot \text{nA/V}^2$ due to the momentum-asymmetric contribution of the LVP. Right: Angular dependence of $\sigma^{(2)}(\omega)$ at $\omega = 2\Delta$. The response remains 2π -periodic but is no longer symmetric under $\theta \rightarrow \theta + \pi$, resulting in unequal lobe amplitudes.

the coupling parameter of the LVP was chosen as $\xi = 10^{-24} \text{ C m}$. In the absence of the LVP the conductivity does not depend on θ . Thus there is no preferred direction. Reversing the field orientation produces identical photocurrents, and the response is determined solely by the intrinsic inversion asymmetry of the RM lattice. The unperturbed bands are exactly spin degenerate, which is handled numerically by introducing a tiny Zeeman splitting that stabilizes the gauge, as discussed in Supplementary Material S2. The results for the raw shift conductivity are shown in Figure 3.

Once the LV contribution $H_{\text{LV}}(k)$ is included, the odd dependence on momentum makes the response sensitive

to the sign of the longitudinal component of the applied static electric field. Since the shift current is governed by the momentum-resolved interband phase, even a small imbalance in $\phi(k)$ between positive and negative crystal momenta produces a measurable contrast between opposite field orientations. We quantify this effect through the difference

$$\Delta\sigma^{(2)}(\omega, \theta) = \sigma^{(2)}(\omega, \theta) - \sigma^{(2)}(\omega, \theta + \pi), \quad (9)$$

shown in Fig. 2(left). The largest contrast appears at $\theta = 0$ and $\theta = \pi$, where the projection of the optical field along the chain is maximal. At the band edge resonance the peak reaches $\Delta\sigma^{(2)}(\omega) = 1.53 \text{ nm} \cdot \text{nA/V}^2$. Since the deformation induced by the LV term scales with the longitudinal projection of the field, the strength of the effect varies smoothly with angle and makes $\sigma^{(2)}(\omega, \theta)$ explicitly angle dependent.

The angular dependence at the bandgap frequency is shown in Fig. 2(right). In the Lorentz-symmetric case the conductivity is flat as a function of θ , consistent with the absence of any mechanism that distinguishes opposite orientations of the applied static electric field. The LVP breaks this π reversal symmetry while preserving the overall 2π periodicity. As θ is rotated from 0 to π , the sign of the longitudinal component $E_x(\theta) = E_0 \cos \theta$ changes, and one finds a clear inequality $\sigma^{(2)}(\omega, 0) < \sigma^{(2)}(\omega, \pi)$. The directions $\theta = \pi/2$ and $3\pi/2$ remain nodal, since in this configuration the longitudinal projection vanishes and the LV term becomes inactive. These null orientations provide an internal check that separates the genuine asymmetry from polarization dependent artifacts or small misalignments.

The same symmetry signatures suggest a practical detection scheme based on a comparison between field ori-

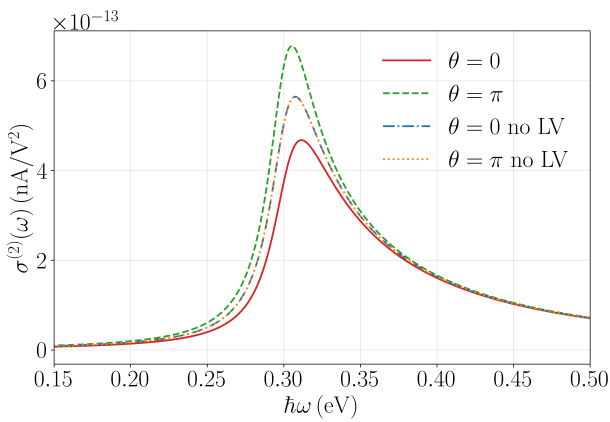


FIG. 3. Shift conductivity $\sigma^{(2)}(\omega)$ for opposite field orientations $\theta = 0$ and $\theta = \pi$. In the absence of LV the responses for θ and $\theta + \pi$ coincide, while the LVP lifts this equivalence and produces a directional asymmetry near the band-edge resonance.

entations separated by π . The proposed geometry, illustrated in Fig. 1, consists of a nanowire or elongated flake contacted along its axis and illuminated by linearly polarized light. By rotating the polarization angle θ , one can monitor how the shift current $\sigma^{(2)}(\omega, \theta)$ changes with the longitudinal projection of the field relative to the fixed background \mathbf{v} . Measurements performed for θ and $\theta + \pi$ give directly the differential photogalvanic response, which isolates the momentum-odd component generated by the LVP. Since the rotation is performed optically, both orientations can be probed without modifying the device alignment. Comparing the results from θ and $\theta + \pi$ therefore cancels contributions that are even under field reversal such as background noise or laser fluctuations, while isolating the odd component of the LVP, thermal offsets, and background photocurrents. Orientations where the field is perpendicular to \mathbf{v} act as internal null points, because the LV contribution vanishes when $E_x(\theta) = 0$.

To estimate the measurable current associated with the LV-induced asymmetry, we express the dc photocurrent difference in terms of the optical intensity at the sample. For a monochromatic drive with linear polarization along the wire axis, the asymmetry scales as $\Delta I \sim \Delta\sigma^{(2)}|E(\omega)|^2$, where $\Delta\sigma^{(2)}$ is the computed conductivity difference and $E(\omega)$ is the optical field amplitude. Writing the time-averaged intensity as $I_{\text{opt}} = \frac{1}{2}nc\varepsilon_0|E(\omega)|^2$ gives

$$\Delta I \simeq \Delta\sigma^{(2)} \frac{2I_{\text{opt}}}{nc\varepsilon_0}. \quad (10)$$

In this one-dimensional geometry, the length-gauge shift-current expression $J = \sigma^{(2)}E^2$ yields a total current rather than a current density, since the transverse dimensions are implicitly absorbed in the definition of $\sigma^{(2)}$. The optical electric-field amplitude is related to the incident intensity by $E^2 = 2I_{\text{opt}}/(nc\varepsilon_0)$, as in the standard formulation of the bulk photovoltaic effect [19]. Using $\Delta\sigma^{(2)} \simeq 2 \times 10^{-22} \text{ A m}^2/\text{V}^2$ and a representative focused intensity $I_{\text{opt}} \sim 10^4 \text{ W/cm}^2$ [25, 44], we obtain $\Delta I \sim 10^{-11}\text{--}10^{-10} \text{ A}$ (tens to hundreds of pA for $n \sim 1$), which is within the resolution of standard low-noise photocurrent measurements [24]. Even for more conservative intensities, the resulting signal remains in the picoampere range, comparable to values reported for nonlinear photoconductivity in low-dimensional materials [24–28]. The magnitude of this current can be further enhanced by increasing the optical intensity, reducing the illumination spot size, or employing modulation and lock-in detection schemes.

Because the measured current asymmetry with E_x is directly proportional to the LVP, a detectable asymmetry can be translated into a sensitivity to the LV coupling ξ . In the present model, the directional shift-current response scales linearly with ξ through the aforementioned effective tilt $\alpha = \hbar\xi E_x/(m_e c)$. Increasing the ap-

plied static field therefore enhances the Lorentz-violating contribution and improves the sensitivity to smaller values of ξ . For the parameters used here, with a static field $E_x = 10^5 \text{ V/m}$, an experimentally resolvable current asymmetry of order 10 pA corresponds to a detectable coupling strength $\xi \sim 10^{-24} \text{ C m}$ [24]. This value should be understood as a sensitivity scale associated with a resolvable field-odd current response, rather than as a fundamental bound.

Conclusion — We have presented an electrically controlled protocol to probe Lorentz-violating signatures in noncentrosymmetric crystalline systems through the nonlinear shift photocurrent. Using a spinful Rice–Mele model, we showed that a stationary LV background generates a momentum-odd correction to the Bloch Hamiltonian, which leaves a direct signature on the interband phase and produces a field-odd contribution to the shift current. As a result, the photocurrent distinguishes opposite orientations of the applied field, breaking the equivalence between θ and $\theta + \pi$. This directional asymmetry can be isolated experimentally by reversing the applied field while keeping the sample geometry fixed, with nodal configurations ($\theta = \pi/2, 2\pi/3$) providing a consistency check. For realistic device dimensions and applied fields, the resulting current contrast lies well within the sensitivity of existing photogalvanic measurements, allowing the corresponding LV coupling ξ to be directly inferred.

Acknowledgments — The authors acknowledge financial support from the Brazilian funding agencies FAPES (1044/2022, 1081/2022 - P:2022-8L35F, and 875/2023 - P:2023-V36VC), and CNPq (under grants 444450/2024-6, 305227/2024-6 and 442781/2023-7) and are also grateful for the computational resources of the SciCom Lab/UFES. We also acknowledge financial support from MICIU/AEI/10.13039/501100011033 through Grants TED2021-131323B-I00 and PID2022-141712NB-C21, the María de Maeztu Program for Units of Excellence in R&D through Grant CEX2023-001316-M, the Comunidad de Madrid within the Recovery, Transformation and Resilience Plan through the project “Disruptive 2D materials” (MAD2D-CM-UAM7) funded by the NextGenerationEU programme from the European Union, and we also thank the Naturgy Foundation. We also acknowledge computational resources from CCC at UAM and Spanish RES.

* wendel.paz@ufes.br, corresponding author

- [1] D. Colladay and V. A. Kostelecký, *Phys. Rev. D* **55**, 6760 (1997).
- [2] D. Colladay and V. A. Kostelecký, *Phys. Rev. D* **58**, 116002 (1998).
- [3] V. A. Kostelecký, *Phys. Rev. D* **69**, 105009 (2004).
- [4] V. A. Kostelecký and N. Russell, *Reviews of Modern*

Physics **83**, 11 (2011).

[5] G. Gabrielse, A. Khabbaz, D. S. Hall, C. Heimann, H. Kalinowsky, and W. Jhe, *Physical Review Letters* **82**, 3198 (1999).

[6] A. A. Abdo, others, and The Fermi LAT and Fermi GBM Collaborations, *Nature* **462**, 331 (2009).

[7] M. G. Aartsen, others, and The IceCube Collaboration, *Nature Physics* **14**, 961 (2018).

[8] M. Ahmadi, others, and The ALPHA Collaboration, *Nature* **541**, 506 (2017).

[9] G. W. Bennett, others, and The Muon (g-2) Collaboration, *Physical Review Letters* **100**, 091602 (2008).

[10] J. B. R. Battat, J. F. Chandler, and C. W. Stubbs, *Physical Review Letters* **99**, 241103 (2007).

[11] N. P. Armitage, E. J. Mele, and A. Vishwanath, *Reviews of Modern Physics* **90**, 015001 (2018).

[12] A. A. Soluyanov, D. Gresch, Z. Wang, Q. Wu, M. Troyer, X. Dai, and B. A. Bernevig, *Nature* **527**, 495 (2015).

[13] A. G. Grushin, *Phys. Rev. D* **86**, 045001 (2012).

[14] A. A. Burkov, *Physical Review Letters* **113**, 187202 (2014).

[15] J. Xiong, S. K. Kushwaha, T. Liang, J. W. Krizan, M. Hirschberger, W. Wang, R. J. Cava, and N. P. Ong, *Science* **350**, 413 (2015).

[16] K. Bakke and H. Belich, *Annalen der Physik* **526**, 187 (2014).

[17] K. Bakke and H. Belich, *Annals of Physics* **354**, 1 (2015).

[18] K. Bakke and H. Belich, *Journal of Physics G: Nuclear and Particle Physics* **42**, 095001 (2015).

[19] J. E. Sipe and A. I. Shkrebtii, *Phys. Rev. B* **61**, 5337 (2000).

[20] S. M. Young and A. M. Rappe, *Physical review letters* **109**, 116601 (2012).

[21] T. Morimoto and N. Nagaosa, *Science Advances* **2**, e1501524 (2016).

[22] M. A. García-Blázquez, J. J. Esteve-Paredes, A. J. Uría-Álvarez, and J. J. Palacios, *Journal of Chemical Theory and Computation* **19**, 9416 (2023).

[23] J. J. Esteve-Paredes, M. A. García-Blázquez, A. J. Uría-Álvarez, M. Camarasa-Gómez, and J. J. Palacios, *npj Computational Materials* **11**, 13 (2025).

[24] G. Xue, Z. Zhou, Q. Guo, Y. Zuo, W. Wei, J. Yang, P. Yin, S. Zhang, D. Zhong, Y. You, X. Sui, C. Liu, M. Wu, H. Hong, Z.-J. Wang, P. Gao, Q. Li, L. Zhang, D. Yu, F. Ding, Z. Wei, C. Liu, and K. Liu, *Science* **384**, 1100 (2024).

[25] Y. J. Zhang, T. Ideue, M. Onga, F. Qin, R. Suzuki, A. Zak, R. Tenne, J. H. Smet, and Y. Iwasa, *Nature* **570**, 349 (2019), publisher: Nature Publishing Group.

[26] Y. Chen, L. Liang, S. Zhang, D. Huang, J. Zhang, S. Xu, C. Liang, and W. Xu, *Nanoscale* **10**, 1622 (2025).

[27] S. Pal, S. Muthukrishnan, B. Sadhukhan, S. N. V., D. Murali, and P. Murugavel, *Journal of Applied Physics* **129**, 084106 (2021).

[28] Y. Li, J. Fu, X. Mao, C. Chen, H. Liu, M. Gong, and H. Zeng, *Nature Communications* **12**, 5896 (2021), publisher: Nature Publishing Group.

[29] M.-M. Yang, D. J. Kim, and M. Alexe, *Science* **360**, 904 (2018).

[30] V. A. Kostelecký and C. Lane, *Physical Review D* **60**, 116010 (1999).

[31] V. A. Kostelecký, R. Lehnert, N. McGinnis, M. Schreck, and B. Seradjeh, *Physical Review Research* **4**, 023106 (2022).

[32] H. Belich, T. Costa-Soares, M. FerreiraJr, and J. Helayél-Neto, *The European Physical Journal C-Particles and Fields* **41**, 421 (2005).

[33] H. Belich, T. Costa-Soares, M. Ferreira, J. Helayél-Neto, and M. Orlando, *The European Physical Journal C* **42**, 127 (2005).

[34] H. Belich, T. Costa-Soares, M. Ferreira, J. Helayél-Neto, and M. Orlando, *Physics Letters B* **639**, 675 (2006).

[35] H. Belich, T. Costa-Soares, M. M. Ferreira, J. A. Helayél-Neto, and F. M. O. Moucherek, *Phys. Rev. D* **74**, 065009 (2006).

[36] S. M. Carroll, G. B. Field, and R. Jackiw, *Phys. Rev. D* **41**, 1231 (1990).

[37] K. Bakke and H. Belich, *Annalen der Physik* **526**, 187 (2014).

[38] M. Rice and E. Mele, *Physical Review Letters* **49**, 1455 (1982).

[39] S. Wang, W. Li, C. Deng, Z. Hong, H.-B. Gao, X. Li, Y. Gu, Q. Zheng, Y. Wu, P. G. Evans, J.-F. Li, C.-W. Nan, and Q. Li, *Nature Communications* **15**, 1374 (2024), publisher: Nature Publishing Group.

[40] T. Hiraoka, S. Nestler, W. Zhang, S. Rossel, H. A. Hafez, S. Fabretti, H. Schlörb, A. Thomas, and D. Turchinovich, *Nature Communications* **16**, 5235 (2025), publisher: Nature Publishing Group.

[41] N. Leisgang, S. Shree, I. Paradiso, L. Sponfeldner, C. Robert, D. Lagarde, A. Balocchi, K. Watanabe, T. Taniguchi, X. Marie, R. J. Warburton, I. C. Gerber, and B. Urbaszek, *Nature Nanotechnology* **15**, 901 (2020), publisher: Nature Publishing Group.

[42] J. Klein, J. Wierzbowski, A. Steinhoff, M. Florian, M. Rösner, F. Heimbach, K. Müller, F. Jahnke, T. O. Wehling, J. J. Finley, and M. Kaniber, *Nano Letters* **17**, 392 (2017), publisher: American Chemical Society.

[43] J. Wang, N. Han, Z.-D. Luo, M. Zhang, X. Chen, Y. Liu, Y. Hao, J. Zhao, and X. Gan, *ACS Nano* **16**, 6404 (2022), publisher: American Chemical Society.

[44] J. Krishna, P. Garcia-Goericela, F. de Juan, and J. Ibañez-Azpiroz, *Physical Review B* **108**, 165418 (2023), publisher: American Physical Society.

**SUPPLEMENTAL MATERIAL FOR:
“NONLINEAR OPTICAL RESPONSE AS A PROBE OF EMERGENT LORENTZ SYMMETRY
VIOLATION IN NONCENTROSYMMETRIC MATERIALS”**

S1. DERIVATION OF THE LORENTZ-VIOLATING HAMILTONIAN CORRECTION

We begin with the gauge-invariant Dirac equation incorporating a non-minimal Lorentz-violating (LV) coupling:

$$(ic\hbar\gamma^\mu\mathcal{D}_\mu - mc^2)\Psi = 0, \quad (\text{S1})$$

with the extended covariant derivative:

$$\mathcal{D}_\mu = \partial_\mu + i\frac{e}{\hbar c}A_\mu + i\frac{g}{\hbar c}v^\nu\tilde{F}_{\mu\nu}, \quad (\text{S2})$$

where $\tilde{F}^{\mu\nu} = \frac{1}{2}\epsilon^{\mu\nu\alpha\beta}F_{\alpha\beta}$ is the dual electromagnetic tensor and $v^\mu = (v^0, \mathbf{v})$ is a fixed background four-vector that breaks Lorentz symmetry.

2. Dirac Spinor Decomposition

To obtain the non-relativistic limit, we write the Dirac spinor as:

$$\Psi = \begin{pmatrix} \phi \\ \chi \end{pmatrix},$$

where ϕ and χ are the large and small components, respectively.

Using the Dirac gamma matrices in the Dirac representation:

$$\gamma^0 = \begin{pmatrix} \mathbb{I} & 0 \\ 0 & -\mathbb{I} \end{pmatrix}, \quad \gamma^i = \begin{pmatrix} 0 & \sigma^i \\ -\sigma^i & 0 \end{pmatrix},$$

we can write the Dirac equation as a coupled system:

$$(E - eV - g\mathbf{v} \cdot \mathbf{B})\phi = \boldsymbol{\sigma} \cdot \left[\mathbf{p} - \frac{e}{c}\mathbf{A} + gv^0\mathbf{B} - g\mathbf{v} \times \frac{\mathbf{E}}{c} \right] \chi + mc^2\phi, \quad (\text{S3})$$

$$(E - eV - g\mathbf{v} \cdot \mathbf{B})\chi = \boldsymbol{\sigma} \cdot \left[\mathbf{p} - \frac{e}{c}\mathbf{A} + gv^0\mathbf{B} - g\mathbf{v} \times \frac{\mathbf{E}}{c} \right] \phi - mc^2\chi. \quad (\text{S4})$$

3. Foldy–Wouthuysen Expansion

In the non-relativistic limit ($E \approx mc^2 + \varepsilon$, with $\varepsilon \ll mc^2$), the small component can be approximated as:

$$\chi \approx \frac{1}{2mc}\boldsymbol{\sigma} \cdot \left(\mathbf{p} - \frac{e}{c}\mathbf{A} + gv^0\mathbf{B} - g\mathbf{v} \times \frac{\mathbf{E}}{c} \right) \phi. \quad (\text{S5})$$

Substituting Eq. (S5) into the upper equation yields the effective Schrödinger-Pauli equation for ϕ :

$$(E - mc^2 - eV - g\mathbf{v} \cdot \mathbf{B})\phi = \frac{1}{2m}(\boldsymbol{\sigma} \cdot \boldsymbol{\Pi})^2\phi, \quad (\text{S6})$$

where the generalized momentum is

$$\boldsymbol{\Pi} = \underbrace{(\mathbf{p} - e\mathbf{A})}_{\boldsymbol{\Pi}_{\text{em}}} + \underbrace{(gv_0\mathbf{B} - g\mathbf{v} \times \mathbf{E})}_{\boldsymbol{\Delta}}. \quad (\text{S7})$$

Throughout this section we set $\hbar = c = 1$.

Using the Pauli identity

$$(\boldsymbol{\sigma} \cdot \boldsymbol{\Pi})^2 = \boldsymbol{\Pi}^2 + \frac{i}{2} \epsilon_{abc} \sigma_c [\Pi_a, \Pi_b],$$

and computing the commutator

$$\begin{aligned} [\Pi_a, \Pi_b] &= [\Pi_{\text{em},a}, \Pi_{\text{em},b}] + [\Pi_{\text{em},a}, \Delta_b] + [\Delta_a, \Pi_{\text{em},b}] \\ &= i \epsilon_{abk} [eB_k + (\boldsymbol{\nabla} \times \boldsymbol{\Delta})_k], \end{aligned} \quad (\text{S8})$$

we obtain

$$(\boldsymbol{\sigma} \cdot \boldsymbol{\Pi})^2 = \boldsymbol{\Pi}^2 - \boldsymbol{\sigma} \cdot [e \mathbf{B} + \boldsymbol{\nabla} \times \boldsymbol{\Delta}]. \quad (\text{S9})$$

Substituting Eq. (S9) into the Pauli equation yields the effective Hamiltonian

$$H = eA_0 + \frac{1}{2m_e} \boldsymbol{\Pi}^2 - \frac{1}{2m_e} \boldsymbol{\sigma} \cdot [e \mathbf{B} + \boldsymbol{\nabla} \times \boldsymbol{\Delta}]. \quad (\text{S10})$$

Using $\boldsymbol{\Pi} = \boldsymbol{\Pi}_{\text{em}} + \boldsymbol{\Delta}$ and $(\mathbf{a} + \mathbf{b})^2 = \mathbf{a}^2 + \{\mathbf{a}, \mathbf{b}\} + \mathbf{b}^2$,

$$H = eA_0 + \frac{1}{2m_e} (\mathbf{p} - e\mathbf{A})^2 - \frac{e}{2m_e} \boldsymbol{\sigma} \cdot \mathbf{B} + \frac{1}{2m_e} \{\boldsymbol{\Pi}_{\text{em}}, \boldsymbol{\Delta}\} + \frac{1}{2m_e} \boldsymbol{\Delta}^2 - \frac{1}{2m_e} \boldsymbol{\sigma} \cdot (\boldsymbol{\nabla} \times \boldsymbol{\Delta}). \quad (\text{S11})$$

For weakly varying fields, $[\mathbf{p}, \boldsymbol{\Delta}] \simeq -i\boldsymbol{\nabla} \cdot \boldsymbol{\Delta}$, and taking $\boldsymbol{\nabla} \cdot \boldsymbol{\Delta} \simeq 0$, the mixed anticommutator gives

$$\frac{1}{2m_e} \{\boldsymbol{\Pi}_{\text{em}}, \boldsymbol{\Delta}\} \simeq \frac{1}{m_e} \boldsymbol{\Delta} \cdot (\mathbf{p} - e\mathbf{A}). \quad (\text{S12})$$

The quadratic and curl terms follow from

$$\boldsymbol{\Delta}^2 = (gv_0 \mathbf{B} - g \mathbf{v} \times \mathbf{E})^2 = g^2 [(v_0)^2 \mathbf{B}^2 - 2v_0 \mathbf{B} \cdot (\mathbf{v} \times \mathbf{E}) + |\mathbf{v} \times \mathbf{E}|^2], \quad (\text{S13})$$

$$\boldsymbol{\nabla} \times \boldsymbol{\Delta} = gv_0 (\boldsymbol{\nabla} \times \mathbf{B}) - g \boldsymbol{\nabla} \times (\mathbf{v} \times \mathbf{E}). \quad (\text{S14})$$

Substituting Eqs. (S12)–(S14) into Eq. (S11) and discarding the $(v_0)^2 \mathbf{B}^2$ term (second order in \mathbf{B}), and g^2 term, we obtain

$$\begin{aligned} H = & \left[\frac{1}{2m_e} (\mathbf{p} - e\mathbf{A})^2 + eA_0 - \frac{e}{2m_e} (\boldsymbol{\sigma} \cdot \mathbf{B}) \right] & + \frac{gv_0}{2m_e} \boldsymbol{\sigma} \cdot (\boldsymbol{\nabla} \times \mathbf{B}) - \frac{g}{2m_e} \boldsymbol{\sigma} \cdot [\boldsymbol{\nabla} \times (\mathbf{v} \times \mathbf{E})] \\ & + \frac{gv_0}{m_e} (\mathbf{p} - e\mathbf{A}) \cdot \mathbf{B} - \frac{g}{m_e} (\mathbf{p} - e\mathbf{A}) \cdot (\mathbf{v} \times \mathbf{E}). \end{aligned} \quad (\text{S15})$$

Setting $\mathbf{A} = \mathbf{0}$ and $\mathbf{B} = \mathbf{0}$ in Eq. (S15), the Hamiltonian reduces to

$$H = \frac{\mathbf{p}^2}{2m_e} + eA_0 - \frac{g}{2m_e} \boldsymbol{\sigma} \cdot [\boldsymbol{\nabla} \times (\mathbf{v} \times \mathbf{E})] - \frac{g}{m_e} \mathbf{p} \cdot (\mathbf{v} \times \mathbf{E}). \quad (\text{S16})$$

We will keep the two g -linear pieces: the *spin* term (curl) and the orbital term (linear in \mathbf{p}). Using the standard identity and assuming charge neutrality ($\boldsymbol{\nabla} \cdot \mathbf{E} = 0$) and constant \mathbf{v} ,

$$\boldsymbol{\nabla} \times (\mathbf{v} \times \mathbf{E}) = \mathbf{v} (\boldsymbol{\nabla} \cdot \mathbf{E}) - (\mathbf{v} \cdot \boldsymbol{\nabla}) \mathbf{E} = -(\mathbf{v} \cdot \boldsymbol{\nabla}) \mathbf{E}. \quad (\text{S17})$$

In momentum space, $\boldsymbol{\nabla} \rightarrow i\mathbf{k}$, hence

$$\boldsymbol{\nabla} \times (\mathbf{v} \times \mathbf{E}) \rightarrow -i(\mathbf{v} \cdot \mathbf{k}) \mathbf{E}. \quad (\text{S18})$$

Our background vector \mathbf{v} is a three-dimensional quantity with components $\mathbf{v} = (v_x, v_y, v_z)$. In what follows, we consider that all components have the same magnitude, i.e., $|v_x| = |v_y| = |v_z| = v$, so that the orientation of \mathbf{v} only determines which interaction channel (spin or orbital) is activated, while its intensity remains fixed.

For a 1D chain along x (Bloch momentum $\mathbf{k} = k \hat{\mathbf{x}}$), choose

$$\mathbf{v} = v \hat{\mathbf{x}}, \quad \mathbf{E} = E_y \hat{\mathbf{y}}. \quad (\text{S19})$$

Then $(\mathbf{v} \cdot \mathbf{k}) = vk$ and $\boldsymbol{\sigma} \cdot \mathbf{E} = E_y \sigma_y$. We will restore factors of \hbar and c at the end for dimensional clarity. From Eq. (S16) and (S18),

$$\delta H_{\text{LV}}^{(\text{spin})}(\mathbf{k}) = -\frac{g}{2m_e} \boldsymbol{\sigma} \cdot [\nabla \times (\mathbf{v} \times \mathbf{E})] \rightarrow \frac{ig}{2m_e} (\mathbf{v} \cdot \mathbf{k}) \boldsymbol{\sigma} \cdot \mathbf{E}. \quad (\text{S20})$$

With the geometry (S19), this is

$$\delta H_{\text{LV}}^{(\text{spin})}(k) = \frac{ig}{2m_e} v k E_y \sigma_y. \quad (\text{S21})$$

On a tight-binding dimer (two-site) chain, the odd-in- k factor comes with the intercell phase and projects onto the sublattice matrix τ_y . Restoring \hbar and c (and absorbing the overall lattice phase so that the coefficient is real), we obtain

$$\delta H_{\text{LV}}^{(\text{spin})}(k) = \frac{\hbar g v E_y}{2m_e c} k \tau_y \otimes \sigma_y. \quad (\text{S22})$$

The orbital g -linear piece in (S16) is

$$\delta H_{\text{LV}}^{(\text{orb})} = -\frac{g}{m_e} \mathbf{p} \cdot (\mathbf{v} \times \mathbf{E}). \quad (\text{S23})$$

For the geometry (S19), the cross product between the background field and the electric field yields $\mathbf{v} \times \mathbf{E} = -v_z E_y \hat{\mathbf{x}}$. This configuration corresponds to the only nonvanishing combination of field directions that couples directly to the crystal momentum along the chain.

$$\delta H_{\text{LV}}^{(\text{orb})} = \frac{g}{m_e} p_x (v_z E_y). \quad (\text{S24})$$

Then, along the chain, $p_x \rightarrow \hbar k$ and the intercell phase projection yields τ_y :

$$\delta H_{\text{LV}}^{(\text{orb})}(k) = \frac{\hbar g v E_y}{m_e c} k \tau_y \otimes \sigma_0. \quad (\text{S25})$$

$\lambda_k \equiv \alpha k$, $\alpha = \hbar \xi E_x / (m_e c)$, $\xi \equiv gv$, the Lorentz-violating lattice Hamiltonian reads

$$H_{\text{LV}}(k) = \lambda_k \left[\frac{1}{2} (\tau_y \otimes \sigma_y) + (\tau_y \otimes \sigma_0) \right]. \quad (\text{S26})$$

S2. SHIFT-CONDUCTIVITY FORMALISM AND NUMERICAL IMPLEMENTATION

The interband dipole matrix elements are evaluated in the length gauge at fixed crystal momentum,

$$r_{mn}(\mathbf{k}) = i \frac{\langle u_m(\mathbf{k}) | \partial_{\mathbf{k}} H(\mathbf{k}) | u_n(\mathbf{k}) \rangle}{E_n(\mathbf{k}) - E_m(\mathbf{k})}, \quad (\text{S27})$$

where $|u_n(\mathbf{k})\rangle$ are the cell-periodic Bloch eigenstates of the full Hamiltonian and $\partial_{\mathbf{k}} H$ is obtained analytically. The diagonal Berry connections are defined as

$$A_{nn}(\mathbf{k}) = i \langle u_n(\mathbf{k}) | \partial_{\mathbf{k}} u_n(\mathbf{k}) \rangle, \quad (\text{S28})$$

and are computed numerically from overlaps between eigenstates at neighboring \mathbf{k} -points.

To ensure numerical smoothness, the phases of the eigenstates are fixed by imposing a continuous gauge across the Brillouin zone. At each \mathbf{k} , we extract

$$\theta_{n\mathbf{k}} = \arg \left[\sum_{\alpha} U_{\alpha n}(\mathbf{k}) \right], \quad (\text{S29})$$

and redefine the eigenvectors as

$$\tilde{u}_n(\mathbf{k}) = e^{-i\theta_{n\mathbf{k}}} u_n(\mathbf{k}), \quad (\text{S30})$$

so that $\sum_{\alpha} \tilde{U}_{\alpha n}(\mathbf{k})$ is real and positive. This procedure enforces a smooth gauge along \mathbf{k} , stabilizing both the Berry connections and the phase of the dipole matrix elements [22, 23].

Writing

$$r_{mn}(\mathbf{k}) = |r_{mn}(\mathbf{k})| e^{i\phi_{mn}(\mathbf{k})}, \quad (\text{S31})$$

the shift conductivity is given in the length gauge by [19]

$$\sigma_{abb}^{(2)}(\omega, \theta) = -\frac{\pi e^3}{\hbar^2} \sum_{m \neq n} \int \frac{dk}{2\pi} f_{mn}(k) |r_{mn}^b(k)|^2 R_{mn}^a(k) \delta(E_{mn}(k) - \omega), \quad (\text{S32})$$

In this expression, $f_{mn}(k) = f_m(k) - f_n(k)$ is the occupation factor. At zero temperature with a fully occupied valence band and an empty conduction band, $f_{mn}(k) = 1$ for all allowed interband transitions, which is the regime used in our numerical evaluation. The parameter sensitive to the perturbation is the shift vector, defined as

$$R_{mn}^a(\mathbf{k}) = \partial_{k_a} \phi_{mn}(\mathbf{k}) - (A_{mm}^a(\mathbf{k}) - A_{nn}^a(\mathbf{k})) \quad (\text{S33})$$

Only the longitudinal component of the static background field, $E_x(\theta) = E_0 \cos \theta$, couples to the Lorentz-violating term $\lambda_k = \alpha k$. This coupling produces a k -odd modification of the interband phase and therefore changes the shift vector $R_{mn}^a(k)$. The phase derivative is evaluated numerically using a symmetric finite-difference form,

$$\partial_k \phi_{mn}(\mathbf{k}) \simeq \frac{1}{2dk} \arg [r_{mn}(\mathbf{k} + dk) r_{mn}(\mathbf{k} - dk)^*], \quad (\text{S34})$$

which depends only on phase differences and is therefore gauge-invariant.